

## Multiorbital model reveals a second-order topological insulator in $1H$ transition metal dichalcogenides

Jiang Zeng<sup>1,2,\*</sup>, Haiwen Liu,<sup>3</sup> Hua Jiang,<sup>4</sup> Qing-Feng Sun,<sup>2,5,6</sup> and X. C. Xie<sup>2,5,6,†</sup>

<sup>1</sup>*School of Physics and Electronics, Hunan University, Changsha 410082, China*

<sup>2</sup>*International Center for Quantum Materials, School of Physics, Peking University, Beijing 100871, China*

<sup>3</sup>*Center for Advanced Quantum Studies, Department of Physics, Beijing Normal University, Beijing 100875, China*

<sup>4</sup>*School of Physical Science and Technology, Soochow University, Suzhou 215006, China*

<sup>5</sup>*Beijing Academy of Quantum Information Sciences, Beijing 100193, China*

<sup>6</sup>*CAS Center for Excellence in Topological Quantum Computation, University of Chinese Academy of Sciences, Beijing 100871, China*



(Received 12 April 2021; accepted 4 October 2021; published 11 October 2021)

Recently, a new class of second-order topological insulators (SOTIs) characterized by an electronic dipole has been theoretically introduced and proposed to host topological corner states. As a novel topological state, it has been attracting great interest and experimentally realized in artificial systems of various fields of physics based on multisublattice models, e.g., breathing kagome lattice. In order to realize such kind of SOTI in natural materials, we proposed a symmetry-faithful multiorbital model. Then, we reveal several familiar transition metal dichalcogenide (TMD) monolayers as a material family of two-dimensional SOTI with large bulk gaps. The topologically protected corner state with fractional charge is pinned at Fermi level due to the charge neutrality and filling anomaly. Additionally, we propose that the zero-energy corner state is preserved in the heterostructure composed of a topological nontrivial flake embedded in a trivial material. The novel second-order corner states in familiar TMD materials hold promise for revealing unexpected quantum properties and applications.

DOI: [10.1103/PhysRevB.104.L161108](https://doi.org/10.1103/PhysRevB.104.L161108)

Topological insulators are materials with gapped band structure characterized by quantized topological invariants that are defined with respect to the symmetries of their bulk Hamiltonian [1,2]. In a  $d$ -dimensional ( $d$ D) topological insulator, a topologically nontrivial bulk band structure implies the existence of  $(d - 1)$ D boundary states. Instead, a  $d$ D second-order topological insulator (SOTI) exhibits  $(d - 2)$ D topological states [3–16]. For example, there are symmetry protected corner states with localized fractional charge in a two-dimensional (2D) SOT—[4,5,7–11,15,16]. In 2017, the concept of higher-order topological insulators is introduced and characterized by quantized multipole [4]. SOTIs and their corner states are investigated in systems with electronic quadruples [8–10,14–16]. Further in 2018, Ezawa further proposed that the electronic dipole could also induce second-order corner states in a breathing kagome model [5,7,17]. This new kind of second-order corner states have been experimentally realized via artificially designing metamaterials in various fields of physics [18–32].

It is appealing to search SOTIs in natural and stable materials, especially the ones have been fabricated through mature technology of high quality, for further study and application [33]. However, experimental demonstration of the existing single-orbital and multisublattice models, e.g., the breathing kagome model, in natural electronic materials is still lacking [24]. It is well known that the electronic bands of a

material are usually contributed from multiorbital, due to the degeneracy nature of the atomic orbitals and the hybridization between them. A multiorbital model would provide a better guidance for realizing intriguing physics in natural materials [34].

Here, we construct a multiorbital model to reveal several familiar transition metal dichalcogenides (TMDs) as a material family of 2D SOTI with a nontrivial bulk electronic dipole. The multiorbital model proposed here shares a similarity to the multisublattice breathing kagome model [5,7] and has special advantages on materials realization. Our first-principles calculations and theoretical analysis show that the  $1H$ - $MX_2$  monolayers with  $M = (\text{W}, \text{Mo})$  and  $X = (\text{Te}, \text{Se}, \text{S})$  are 2D SOTIs with nontrivial electronic dipoles  $\mathbf{P} = (\frac{1}{3}, \frac{2}{3})$  and large band gaps about 2 eV, while some other insulators, for example,  $1H$ - $\text{TiS}_2$ , are topologically trivial. In the topologically nontrivial phase, the Wannier center of the occupied state locates on neither the  $M$  nor the  $X$  atom sites. The mismatch between the Wannier center of electron and the atom sites refers to an electronic dipole that is quantized and protected by the  $C_3$  rotation symmetry. Using a topological nontrivial  $\text{MoS}_2$  flake as a typical example, our calculations and analysis demonstrate the in-gap corner state with localized fractional  $-\frac{1}{3}|e|$  charges. Additionally, the zero-energy corner state can be protected from edge deformation and environmental implication in the heterostructure composed of a  $\text{MoS}_2$  flake embedded in a trivial  $\text{TiS}_2$  monolayer.

Monolayers TMD- $MX_2$  with  $M = (\text{W}, \text{Mo})$  and  $X = (\text{Te}, \text{Se}, \text{S})$  possess a variety of polytypic structures. The most-studied  $1H$  structure has the  $D_{3h}$  point-group symmetry and

\*Corresponding author: zengjiang@pku.edu.cn

†Corresponding author: xcxie@pku.edu.cn

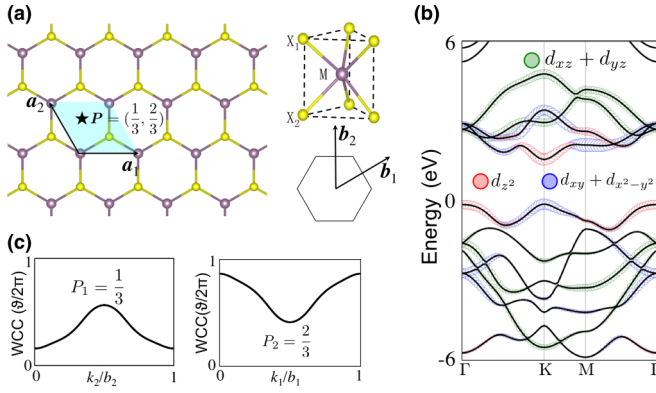


FIG. 1. Atomic structure and electronic structure of a  $1H-MX_2$  monolayer.  $M$  stands for (W, Mo) and  $X$  stands for (Te, Se, S). (a) Atomic structure of a  $1H-MX_2$  monolayer. The arrows  $\mathbf{a}_1$  and  $\mathbf{a}_2$  ( $\mathbf{b}_1$  and  $\mathbf{b}_2$ ) are the two (reciprocal) lattice vectors. One rhombic unit cell is colored in cyan. The star marks the Wannier charge located at the hollow site in the unit cell, corresponding to an electronic dipole  $\mathbf{P} = (\frac{1}{3}, \frac{2}{3})$ . The black hexagon in the lower right corner is the first Brillouin zone. (b) Orbital projected band structure of a  $1H-MoS_2$  monolayer. Colored circles represent contributions from different  $M-d$  orbitals. The Fermi energy  $E_F$  is set to be zero as a reference. (c) Wilson loop of WCC of the highest valence band showing the calculated electronic dipole  $\mathbf{P} = (\frac{1}{3}, \frac{2}{3})$ .

is a sandwich of three planes of 2D hexagonally packed atoms,  $X-M-X$ , as shown in Fig. 1(a). It has been known that the  $1H$  structure in  $MX_2$  is typically stable in free-standing conditions, which is the subject of our work. These  $1H-MX_2$  materials have been experimentally fabricated of high quality [33,35].

The electronic structures of various  $1H-MX_2$  monolayers were obtained by first-principles calculations. Figure 1(b) shows a typical band structure of  $1H-MX_2$  using a  $1H-MoS_2$  monolayer as an example, and the results of the other five compounds are shown in Supplemental Material Fig. S1 [36]. The  $1H-MoS_2$  is an insulator with a fundamental gap of about 2 eV. From early theoretical studies [37], we know that the Bloch states of a  $MoS_2$  monolayer near the band edges for both conduction and valence bands mostly consist of Mo- $d$  orbitals with no hybridization between the  $d_{z^2}$ ,  $d_{xy}$ ,  $d_{x^2-y^2}$  orbitals and  $d_{xz}$ ,  $d_{yz}$  orbitals, which is explicitly shown in Fig. 1(b). With respect to the symmetry consideration, it is reasonable to construct a multi-orbital tight-binding model of monolayer  $MX_2$  using the minimal set of  $M-d_{z^2}$ ,  $d_{xy}$ , and  $d_{x^2-y^2}$  orbitals as basis [37]. Here we construct a simplified while symmetry faithful Hamiltonian  $H_s$  as

$$H_s = \sum_{r,i;j;k} \frac{t_{23} + t_{32} \pm (t_{23} - t_{32})\epsilon_{ijk}}{2} d_{r,i}^\dagger d_{r\pm\mathbf{a}_k,j} |\epsilon_{ijk}| + t_E \sum_{r,i;j} d_{r,i}^\dagger d_{r,j}, \quad (1)$$

where the hopping parameters for different  $1H-MX_2$  monolayers are listed in Table I. It notes that the indirect interaction mediated by the  $X$  atoms is reflected in the difference between  $t_{23}$  and  $t_{32}$ , which breaks the inversion symmetry. Figure 2(a) is a schematic diagram of the above multi-orbital model, which

TABLE I. Hopping parameters in units of eV for the six  $1H-MX_2$  monolayers and calculated electronic dipole  $\mathbf{P}$ .

	MoS <sub>2</sub>	WS <sub>2</sub>	MoSe <sub>2</sub>	WSe <sub>2</sub>	MoTe <sub>2</sub>	WTe <sub>2</sub>
$t_E$	-0.353	-0.382	-0.382	-0.412	-0.456	-0.499
$t_{32}$	-0.922	-1.159	-0.788	-0.987	-0.626	-0.772
$t_{23}$	0.122	0.210	0.065	0.139	0.022	0.099
$\mathbf{P}$	$(\frac{1}{3}, \frac{2}{3})$					

shares a similarity to the multisublattice breathing kagome model [5,7]. See Supplemental Material [36] for more detailed information [37–46].

The electronic dipole can be calculated as [47–49]

$$\mathbf{P} = \frac{1}{S} \int_{BZ} \text{Tr}(\mathbf{A}) d^2\mathbf{k}, \quad (2)$$

where  $\mathbf{A} = -i\langle\Psi|\partial_{\mathbf{k}}|\Psi\rangle$  is the Berry connection for all the valence bands,  $S$  is the area of the Brillouin zone (BZ), and the integration is over the first BZ. The two elements  $P_1$  and  $P_2$  are actually the average values of Wannier charge center (WCC) along the two reciprocal lattice vectors  $\mathbf{b}_2$  and  $\mathbf{b}_1$ , respectively, with the values module 1 confined in the range of [0,1] [47–49]. The location of Wannier center in real space is  $P_1\mathbf{a}_1 + P_2\mathbf{a}_2$  [47–49]. For the multi-orbital model here, the electronic dipole  $\mathbf{P}$  is determined by the WCC of the lowest band that is also the highest valence band and decoupled from other bands.

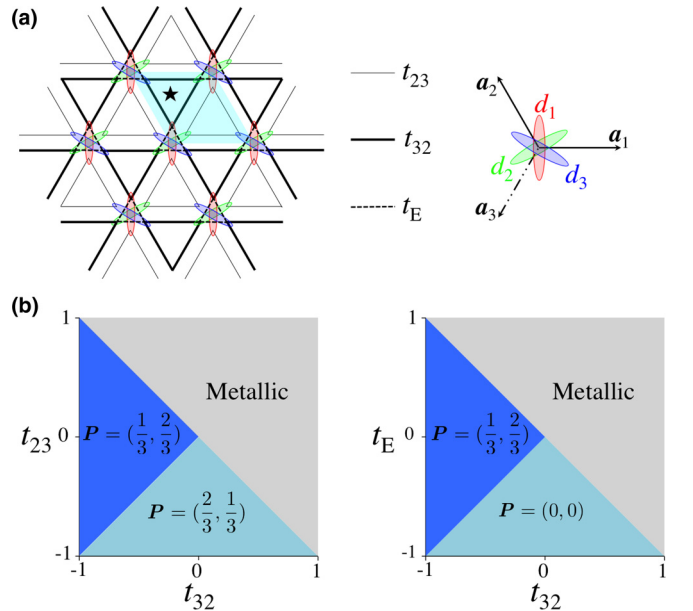


FIG. 2. Schematic lattice diagram and phase diagram of the simplified multi-orbital model Eq. (1). In (a), the three ellipses in different colors represent three orbitals on the same site. The thicker and thinner lines present two different kinds of nearest-neighbor hoppings. The dashed lines present the crystal field effects. The star marks the Wannier charge located at the center of the thicker triangle, corresponding to an electronic dipole  $\mathbf{P} = (\frac{1}{3}, \frac{2}{3})$ . Topological phase diagrams of the multi-orbital model for the (b)  $t_E = 0$  and (c)  $t_{23} = 0$  cases.

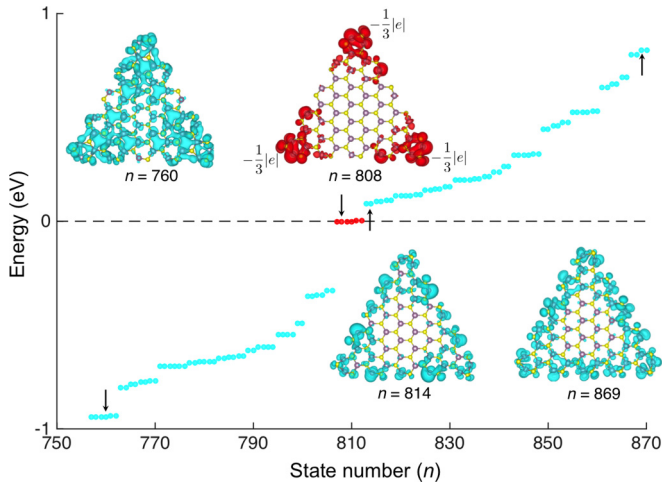


FIG. 3. Energy spectrum of a triangular  $\text{MoS}_2$  flake with armchair edges. The red dots on the Fermi level represent the six in-gap corner states. Other bulk and edge states are colored in cyan. The atomic structure and the charge distribution of the corner state  $n = 808$ , bulk state  $n = 760$ , and edge states  $n = 814$  and  $869$  are shown in the inset. For the corner state  $n = 808$ , the electron is localized and equally distributed on the three corners with  $-\frac{1}{3}|e|$  charge on each corner.

Since a  $1H\text{-MX}_2$  structure shown in Fig. 1(a) has the  $D_{3h}$  point-group symmetry, the electronic dipole must be quantized as  $\mathbf{P} = (0, 0)$ ,  $(\frac{2}{3}, \frac{1}{3})$ , or  $(\frac{1}{3}, \frac{2}{3})$  [49], corresponding to a Wannier charge centered on the  $M$  site,  $X$  site, or hollow site, respectively. The calculated electronic dipole is  $\mathbf{P} = (\frac{1}{3}, \frac{2}{3})$  for a  $1H\text{-MoS}_2$  monolayer corresponding to a Wannier charge located on the hollow site. The Wilson loop of WCC of the highest valence band along the two reciprocal lattice vectors is shown in Fig. 1(c). It is a kind of topologically nontrivial polarization when the Wannier charge dislocates from the  $M$  or  $X$  atom sites. It notes that the mismatch between the Wannier center and the atom site is gauge invariant, though the calculated value  $\mathbf{P}$  depends on the choice of the unit cell [5,47–49]. Figure 2(a) provides an intuitive diagram of the multiorbital model showing the Wannier charge locates at the center of the thicker triangle formed by larger hoppings ( $|t_{32}|$ ). In Fig. 2(b), we plot phase diagrams of the multiorbital model of Eq. (1). It shows that the system is nontrivial with  $\mathbf{P} = (\frac{1}{3}, \frac{2}{3})$  when the  $t_{32}$  has a negative value and its amplitude is larger than other hopping parameters. The first-principles calculations and combined theoretical analysis show that all six  $1H\text{-MX}_2$  monolayers with  $M = (\text{W}, \text{Mo})$  and  $X = (\text{Te}, \text{Se}, \text{S})$  are topologically nontrivial with  $\mathbf{P} = (\frac{1}{3}, \frac{2}{3})$ . This topologically nontrivial polarization is expected to produce the zero-energy boundary state at the corner and the filling anomaly due to the coexistence of the  $C_3$  rotation symmetry and the charge neutrality [5,7,49].

To explicitly show the zero-energy corner state, a triangular flake of  $1H\text{-MoS}_2$  with armchair edges is constructed, as shown in Fig. 3. There are 45 unit cells in the triangular  $1H\text{-MoS}_2$  flake and the length of an edge is five hexagons. The triangular shape is chosen to keep the  $C_3$  rotation symmetry which is important for the degeneracy of the corner states. It notes that the appearance of the corner state is sensitive

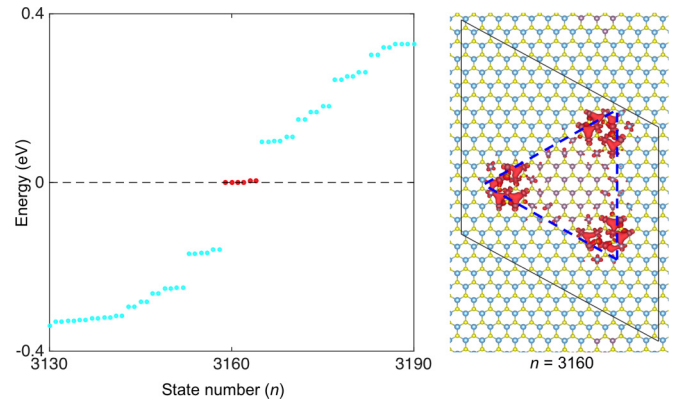


FIG. 4. Energy spectrum of a heterostructure composed of a triangular  $\text{MoS}_2$  flake in a  $\text{TiS}_2$  monolayer. In (a), the red dots on the Fermi level represent the six in-gap corner states. (b) The charge distribution of corner state  $n = 3160$ . The electron is localized and equally distributed on the three corners with  $-\frac{1}{3}|e|$  charges on each corner.

to the choice of the edge geometry for a topological system protected by spatial symmetry. Previous works have shown that a zigzag edge of  $\text{MoS}_2$  has metallic edge states while an armchair edge is insulating [50,51]. It can be understood in terms of electronic polarization. Since polarization  $\mathbf{P}$  is perpendicular to the zigzag direction, metallic edge states are expected due to the charge accumulation at the zigzag edge. In contrast, no such charge accumulation and metallic states at the armchair edges exist that are parallel to  $\mathbf{P}$ . A flake with insulating armchair edges is a better choice for the observation of in-gap corner states.

The first-principles calculated electronic spectrum of the  $1H\text{-MoS}_2$  flake is shown in Fig. 3. There are six corner states at the Fermi level with three corner states for each spin. In our calculations, both spin degeneracy and spin-orbit coupling are taken into consideration. It notes that the spin-orbit coupling does not split the spin degeneracy of the corner states since time-reversal symmetry is preserved. As an example, the charge distribution of the corner state numbered as  $n = 808$  is shown in red. The charge distribution of bulk state  $n = 760$ , edge states  $n = 814$ , and  $n = 869$  are presented in cyan for comparison. For a corner state, one electron is equally distributed on the three corners with  $-\frac{1}{3}|e|$  charges on each corner. By counting the number of electrons in a charge-neutral flake, the six corner states are occupied by four electrons at the Fermi level. When the corner states are unoccupied as a result of filling anomaly [7], there will be  $\frac{4}{3}|e|$  charges at each corner.

Though the corner state is symmetry protected, the degeneracy of the corner state and the fractional charge nature may deviate from the ideal case when the  $C_3$  rotation symmetry is destroyed via edge deformation or external influence [7,18,22–24]. It is expected that edges and corners can be protected via embedding the topological  $1H\text{-MoS}_2$  flake in a trivial material as a heterostructure. Figure 4 shows a typical heterostructure of a triangular  $1H\text{-MoS}_2$  flake in a  $1H\text{-TiS}_2$  monolayer. It notes that the two materials share similar structures as well as lattice parameters. In contrast, the  $1H\text{-TiS}_2$  monolayer is a topologically trivial insulator because

it has two fewer valence electrons per unit cell less than that of the  $1H$ - $\text{MoS}_2$  monolayer [33,35]. We further checked that the  $\text{MoS}_2/\text{TiS}_2$  lateral heterostructure is insulating at the armchair boundary. Thus, a  $1H$ - $\text{TiS}_2$  monolayer provides a perfect platform to protect a topological  $1H$ - $\text{MoS}_2$  flake and its in-gap corner states. As shown in Fig. 4, the six corner states and their fractional charge nature are preserved in the heterostructure. The six corner states are occupied by four electrons at the Fermi level, which is the same as the freestanding flake case.

We reveal several familiar TMD monolayers as a realistic material family of 2D SOTIs. The topologically protected corner state is pinned at the Fermi level due to the charge neutrality and filling anomaly. A multiorbital model is proposed to reveal these TMDs as SOTIs. Additionally, we propose that the zero-energy corner state of a topologically nontrivial flake

can be further protected from edge deformation and environmental implication via embedding it in a trivial material using the  $\text{MoS}_2/\text{TiS}_2$  heterostructure as a typical example. The novel second-order corner state in familiar TMD materials holds promise for revealing unexpected quantum properties and applications.

The authors thank Wei Qin, Ming Lu, and Maoyuan Wang for helpful discussions. This work was supported by the National Basic Research Program of China (2015CB921102 and 2019YFA0308403), the National Natural Science Foundation of China (11674028 and 11822407), the Strategic Priority Research Program of Chinese Academy of Sciences (Grant No. XDB28000000), China Postdoctoral Science Foundation (2020M670011), and the Fundamental Research Funds for the Central Universities.

- 
- [1] X.-L. Qi and S.-C. Zhang, *Rev. Mod. Phys.* **83**, 1057 (2011).
- [2] M. Z. Hasan and C. L. Kane, *Rev. Mod. Phys.* **82**, 3045 (2010).
- [3] J. Langbehn, Y. Peng, L. Trifunovic, F. von Oppen, and P. W. Brouwer, *Phys. Rev. Lett.* **119**, 246401 (2017).
- [4] W. A. Benalcazar, B. A. Bernevig, and T. L. Hughes, *Science* **357**, 61 (2017).
- [5] M. Ezawa, *Phys. Rev. Lett.* **120**, 026801 (2018).
- [6] F. Schindler, A. M. Cook, M. G. Vergniory, Z. Wang, S. S. Parkin, B. A. Bernevig, and T. Neupert, *Sci. Adv.* **4**, eaat0346 (2018).
- [7] W. A. Benalcazar, T. Li, and T. L. Hughes, *Phys. Rev. B* **99**, 245151 (2019).
- [8] Z. Wang, B. J. Wieder, J. Li, B. Yan, and B. A. Bernevig, *Phys. Rev. Lett.* **123**, 186401 (2019).
- [9] X.-L. Sheng, C. Chen, H. Liu, Z. Chen, Z.-M. Yu, Y. X. Zhao, and S. A. Yang, *Phys. Rev. Lett.* **123**, 256402 (2019).
- [10] Y. Ren, Z. Qiao, and Q. Niu, *Phys. Rev. Lett.* **124**, 166804 (2020).
- [11] F. Tang, H. C. Po, A. Vishwanath, and X. Wan, *Nature (London)* **566**, 486 (2019).
- [12] C. Hu, V. Michaud-Rioux, W. Yao, and H. Guo, *Phys. Rev. Lett.* **121**, 186403 (2018).
- [13] S. Jolad and J. K. Jain, *Phys. Rev. Lett.* **102**, 116801 (2009).
- [14] E. Lee, R. Kim, J. Ahn, and B.-J. Yang, *npj Quantum Mater.* **5**, 1 (2020).
- [15] M. J. Park, Y. Kim, G. Y. Cho, and S. B. Lee, *Phys. Rev. Lett.* **123**, 216803 (2019).
- [16] B. Liu, L. Xian, H. Mu, G. Zhao, Z. Liu, A. Rubio, and Z. F. Wang, *Phys. Rev. Lett.* **126**, 066401 (2021).
- [17] M. Ezawa, *Phys. Rev. B* **98**, 045125 (2018).
- [18] X. Ni, M. Weiner, A. Alu, and A. B. Khanikaev, *Nat. Mater.* **18**, 113 (2019).
- [19] S. Imhof, C. Berger, F. Bayer, J. Brehm, L. W. Molenkamp, T. Kiessling, F. Schindler, C. H. Lee, M. Greiter, T. Neupert *et al.*, *Nat. Phys.* **14**, 925 (2018).
- [20] J. Noh, W. A. Benalcazar, S. Huang, M. J. Collins, K. P. Chen, T. L. Hughes, and M. C. Rechtsman, *Nat. Photon.* **12**, 408 (2018).
- [21] M. Serra-Garcia, V. Peri, R. Süsstrunk, O. R. Bilal, T. Larsen, L. G. Villanueva, and S. D. Huber, *Nature (London)* **555**, 342 (2018).
- [22] C. W. Peterson, W. A. Benalcazar, T. L. Hughes, and G. Bahl, *Nature (London)* **555**, 346 (2018).
- [23] C. W. Peterson, T. Li, W. A. Benalcazar, T. L. Hughes, and G. Bahl, *Science* **368**, 1114 (2020).
- [24] S. Kempkes, M. Slot, J. van Den Broeke, P. Capiod, W. Benalcazar, D. Vanmaekelbergh, D. Bercioux, I. Swart, and C. M. Smith, *Nat. Mater.* **18**, 1292 (2019).
- [25] H. Xue, Y. Yang, F. Gao, Y. Chong, and B. Zhang, *Nat. Mater.* **18**, 108 (2019).
- [26] X. Zhang, H.-X. Wang, Z.-K. Lin, Y. Tian, B. Xie, M.-H. Lu, Y.-F. Chen, and J.-H. Jiang, *Nat. Phys.* **15**, 582 (2019).
- [27] A. El Hassan, F. K. Kunst, A. Moritz, G. Andler, E. J. Bergholtz, and M. Bourennane, *Nat. Photon.* **13**, 697 (2019).
- [28] S. Mittal, V. V. Orre, G. Zhu, M. A. Gorlach, A. Poddubny, and M. Hafezi, *Nat. Photon.* **13**, 692 (2019).
- [29] B.-Y. Xie, G.-X. Su, H.-F. Wang, H. Su, X.-P. Shen, P. Zhan, M.-H. Lu, Z.-L. Wang, and Y.-F. Chen, *Phys. Rev. Lett.* **122**, 233903 (2019).
- [30] H. Fan, B. Xia, L. Tong, S. Zheng, and D. Yu, *Phys. Rev. Lett.* **122**, 204301 (2019).
- [31] A. Cerjan, M. Jürgensen, W. A. Benalcazar, S. Mukherjee, and M. C. Rechtsman, *Phys. Rev. Lett.* **125**, 213901 (2020).
- [32] Y. Yang, Z. Jia, Y. Wu, R.-C. Xiao, Z. H. Hang, H. Jiang, and X. Xie, *Sci. Bull.* **65**, 531 (2020).
- [33] J. Li, P. Song, J. Zhao, K. Vaklinova, X. Zhao, Z. Li, Z. Qiu, Z. Wang, L. Lin, M. Zhao *et al.*, *Nat. Mater.* **20**, 181 (2021).
- [34] J. Zeng, M. Lu, H. Liu, H. Jiang, and X. C. Xie, *Sci. Bull.* **66**, 765 (2021).
- [35] M. Chhowalla, H. S. Shin, G. Eda, L.-J. Li, K. P. Loh, and H. Zhang, *Nat. Chem.* **5**, 263 (2013).
- [36] See Supplemental Material at <http://link.aps.org/supplemental/10.1103/PhysRevB.104.L161108> for more electronic structures and model fitting.
- [37] G.-B. Liu, W.-Y. Shan, Y. Yao, W. Yao, and D. Xiao, *Phys. Rev. B* **88**, 085433 (2013).
- [38] W. Kohn and L. J. Sham, *Phys. Rev.* **140**, A1133 (1965).
- [39] G. Kresse and J. Furthmüller, *Comput. Mater. Sci.* **6**, 15 (1996).
- [40] G. Kresse and J. Furthmüller, *Phys. Rev. B* **54**, 11169 (1996).
- [41] P. E. Blöchl, *Phys. Rev. B* **50**, 17953 (1994).
- [42] J. P. Perdew, K. Burke, and M. Ernzerhof, *Phys. Rev. Lett.* **77**, 3865 (1996).

- [43] D. C. Langreth and M. J. Mehl, *Phys. Rev. B* **28**, 1809 (1983).
- [44] A. D. Becke, *Phys. Rev. A* **38**, 3098 (1988).
- [45] H. J. Monkhorst and J. D. Pack, *Phys. Rev. B* **13**, 5188 (1976).
- [46] A. A. Mostofi, J. R. Yates, Y.-S. Lee, I. Souza, D. Vanderbilt, and N. Marzari, *Comput. Phys. Commun.* **178**, 685 (2008).
- [47] A. Alexandradinata, X. Dai, and B. A. Bernevig, *Phys. Rev. B* **89**, 155114 (2014).
- [48] D. Vanderbilt and R. D. King-Smith, *Phys. Rev. B* **48**, 4442 (1993).
- [49] C. Fang, M. J. Gilbert, and B. A. Bernevig, *Phys. Rev. B* **86**, 115112 (2012).
- [50] P. Cui, J.-H. Choi, W. Chen, J. Zeng, C.-K. Shih, Z. Li, and Z. Zhang, *Nano Lett.* **17**, 1097 (2017).
- [51] M. V. Bollinger, J. V. Lauritsen, K. W. Jacobsen, J. K. Nørskov, S. Helveg, and F. Besenbacher, *Phys. Rev. Lett.* **87**, 196803 (2001).